Mode spectra of thermally excited two-dimensional dust Coulomb clusters

A. Melzer*
Institut für Experimentelle und Angewandte Physik, Christian-Albrechts-Universität Kiel, 24098 Kiel, Germany
(Received 26 July 2002; published 31 January 2003)

The mode spectra of finite Coulomb clusters, confined systems of charged microspheres in a complex plasma, have been determined experimentally. The spectral power density of all possible modes has been measured for particle numbers between $N=3$ and $N=145$ under different plasma conditions. The agreement between measured and calculated mode frequencies is found to be very good. From this, the parameters of the particle interaction, like particle charge and screening strength, have been extracted quantitatively. In addition, the particle and mode temperatures have been obtained. The modes and the particles show the same temperature and the principle of equipartitition holds for these systems. Moreover, certain modes of interest have been compared among the different clusters, as there are the breathing mode and intershell rotation as well as the lowest- and highest-frequency modes. Moreover, the mode-integrated spectrum shows two broad maxima which are explained from ''shearlike'' or ''compressionlike'' modes. From this analysis, the transition from finite number to crystal-like properties is observed to occur around $N=12$ particles. Finally, a model to visualize the transition from normal mode oscillations to wave dispersions in a 2D lattice has been proposed.

DOI: 10.1103/PhysRevE.67.016411 PACS number(s): 52.27.Lw, 36.40.Sx

I. INTRODUCTION

Waves and oscillations as fundamental dynamic processes allow to reveal the underlying mechanisms of particle interaction in weakly and strongly coupled complex plasmas. For that reason, a large number of theoretical and experimental investigations have addressed the question of waves and oscillations (see Ref. [1], and references therein). Most of these investigations have been performed in extended two- or three-dimensional (2D or 3D) dust clouds. Bounded systems, so called 2D finite Coulomb clusters, also provide an ideal tool to study the dynamics of complex plasmas and, due the small number of particles involved, are ideally suited for comparison with detailed modeling. The dynamic properties of these finite systems are described in terms of normal modes rather than waves.

Laboratory complex plasmas typically consist of microspheres immersed in a gaseous plasma discharge. The microspheres attain high negative charges of the order of 10^4 elementary charges. Under these conditions the electrostatic energy of neighboring particles by far exceeds their thermal energy, the system is said to be strongly coupled and Coulomb crystallization of the charged particles can occur. The involved space and time scales are perfect for video microscopy and, in addition, dynamical processes are only weakly damped. This makes complex plasmas an ideal system for the study of strongly coupled plasmas and condensed matter.

Two-dimensional finite dust clusters are formed from a small number of particles $N=1-150$ trapped in the space charge sheath above the lower electrode. There the electric field forces can levitate the microspheres against gravity. Since the electric field is increasing from the sheath edge towards the electrode a unique vertical equilibrium position exists forcing the microspheres into a single vertical layer. Horizontally, the particles are confined by a shallow parabolic potential well. The particles arrange in concentric shells forming a ''periodic table'' of 2D clusters (Ref. [2], see also Fig. 1). The structural configuration of the Coulomb clusters is usually given in the form $(N_1,N_2,\ldots)$, where N_1 is the number of particles in the first (innermost) ring, N_2 is that of the second ring, etc.

The 2D clusters are characterized by their total energy

$$E=\frac{1}{2}m\omega_0^2\sum_{i=1}^{N} r_i^2+\frac{Z^2e^2}{4\pi\epsilon_0}\sum_{i>j}^{N}\frac{1}{r_{ij}}\exp\left(-\frac{r_{ij}}{\lambda_D}\right), \qquad (1)$$

which is the sum of the radial (horizontal) confining potential energy and the (screened) Coulomb interaction between the particles [2,3]. Here, m denotes the mass of the particles and Z is their charge number. The strength of the confining potential is denoted by ω_0. In addition, $r_i=(x_i^2+y_i^2)^{1/2}$ is the radial coordinate of the ith particle and $r_{ij}=|\vec{r}_i-\vec{r}_j|$ is the distance between particle i and j.

Using normalized units, $r/r_0\rightarrow r$ and $E/E_0\rightarrow E$, with

$$r_0=\left[\frac{Z^2e^2}{4\pi\epsilon_0}\frac{2}{m\omega_0^2}\right]^{1/3}, \quad E_0=\left[\left(\frac{Z^2e^2}{4\pi\epsilon_0}\right)^2\frac{m\omega_0^2}{2}\right]^{1/3} \qquad (2)$$

together with the screening strength

$$\kappa=\frac{r_0}{\lambda_D}, \qquad (3)$$

the total energy simplifies to

$$E=\sum_{i=1}^{N} r_i^2+\sum_{i>j}^{N}\frac{1}{r_{ij}}\exp(-\kappa r_{ij}). \qquad (4)$$

The normal modes of the 2D clusters are then calculated from the dynamical matrix

*Electronic address: melzer@physik.uni-kiel.de

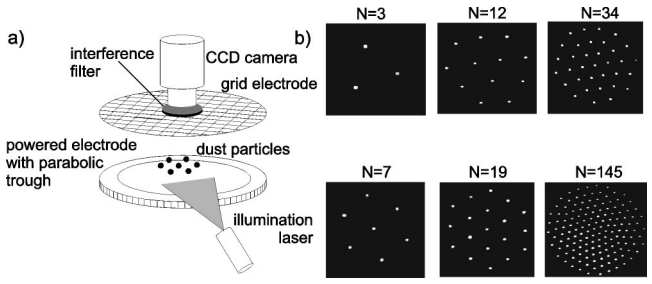

FIG. 1. (a) Scheme of the experimental setup. (b) Snapshots of the clusters with $N=3$, 7, 12, 19, 34, and 145 particles.

$$E_{\alpha\beta,ij}=\frac{\partial^2 E}{\partial r_{\alpha,i}\partial r_{\beta,j}} \tag{5}$$

with α and $\beta=x,y$ and i,j denoting the particle number. The normal mode frequencies ω_ℓ of the $2N$ modes are the eigenvalues of the dynamical matrix (in units of $\omega_0/\sqrt{2}$) and its eigenvectors describe the mode oscillation patterns [3].

For the case of pure Coulomb interaction ($\kappa=0$) there are three normal modes that are independent of the particle number N [3]: (i) the rotation of the entire cluster around the center of the confinement at $\omega=0$, (ii) the (twofold degenerate) sloshing oscillation of the center of mass of the cluster in the horizontal potential well at $\omega=\omega_0$, and (iii) a coherent radial oscillation of all particles, the so called breathing mode, at $\omega=\sqrt{3}\,\omega_0$. For screened interaction ($\kappa>0$), the frequency of the first two modes is unaffected since they do not involve a relative particle motion. In contrast, the frequency of the breathing mode and all other modes becomes dependent on κ and on the particle number N.

The structure, dynamics, and phase transitions of 2D Coulomb clusters with Coulomb or other types of interaction have been extensively studied theoretically [2–4]. Experimentally, the structure of dust Coulomb clusters [5,6] as well as dynamic phenomena [6,7] have been investigated. In these recent cluster experiments, certain modes have been selectively excited by active external disturbances applied to the system. Klindworth *et al.* [6] have stimulated the intershell rotation of $N=19$ and $N=20$ clusters by a pair of laser beams, and Melzer *et al.* [7] have analyzed the breathing and ''antisymmetric'' modes in clusters with $N=3$, 4, and 7 particles by a pulselike modulation of the discharge power.

Here, simultaneous measurements of *all* the possible normal modes of finite clusters are presented. The normal mode spectra are derived purely from the thermal Brownian motion of the microspheres in the cluster. This technique, previously used in experiments by Nunomura *et al.* [8] on waves in ''infinite'' 2D plasma crystals, has been adapted here for finite clusters. The normal mode spectra of different clusters ranging from $N=3$ to $N=145$ under various plasma conditions have been measured. In addition, different configuration states $(N_1,N_2,\ldots)$ have been investigated for some particle numbers. The investigations were focused on the energy (temperature) of the different modes and the effective particle interaction derived from these modes. In addition, special modes have been collated between different cluster sizes and configurations and have been compared to theoretical predictions. Finally, the modes have been classified according to their shear and compressional contribution and a model for the transition from the normal mode in finite clusters to waves in extended crystals is proposed.

II. EXPERIMENT

The experiments have been performed in a parallel plate rf discharge operated in argon at 13.56 MHz with gas pressures of 1.5–4 Pa and discharge powers between 3 and 40 W [see Fig. 1(a)]. A few ($N=3$–150) melamine-formaldehyde particles of 9.55-μm diameter and a mass of $m=6.90\times10^{-13}$ kg are immersed into the plasma and are illuminated by a laser fan (at 690 nm, 40 mW). The particles form 2D finite Coulomb clusters above the lower electrode [see Fig. 1(b)]. The horizontal confinement for the particles is realized by a shallow circular parabolic trough in the electrode. The particle motion is viewed from top and from the side with video cameras and stored into the computer for further processing. In the experiment, it was confirmed from the side view camera that the microspheres are indeed trapped into only a single layer.

The particle motion was recorded from top for typically 1 min, corresponding to 1500 frames at 25 frames per second. No excitation in any form was applied, only the thermal Brownian motion of the particles around their equilibrium positions $\vec{r}_i(t)$ (index i corresponds to the particle number) was recorded.

These thermal fluctuations were used to obtain the normal mode spectra in the following manner: First, the particle velocities $\vec{v}_i(t)=\Delta\vec{r}_i(t)/\Delta t$ were obtained, where $\Delta t=0.04$ s corresponds to the temporal resolution of the camera. Second, the time series of the particle velocities was projected onto the direction of the normal mode vectors for each mode number $\ell=1,\ldots,2N$. That means the quantity

$$v_\ell(t)=\sum_{i=1}^{N}\vec{v}_i(t)\cdot\vec{e}_{i,\ell} \tag{6}$$

was calculated. Here, $\vec{e}_{i,\ell}$ is the eigenvector of particle i for mode number ℓ describing its oscillation amplitude and direction of oscillation. Thus, $v_\ell(t)$ is the contribution of the thermal fluctuations to mode number ℓ in the time domain. Finally, the normal mode spectra of each mode are calculated in form of the spectral power density

$$S_\ell(\omega)=\frac{2}{T}\left|\int_{-T/2}^{T/2}v_\ell(t)\exp(-i\omega t)dt\right|^2. \tag{7}$$

Thus from a single measurement of the thermal particle trajectories the mode spectrum of each mode $\ell=1,\ldots,2N$ are derived.

In the experimental analysis of Nunomura *et al.* [8] on waves in extended 2D crystals a similar technique was introduced, but there the particle motion was projected on the wave vectors $\vec{k}_\parallel,\vec{k}_\perp$ parallel and perpendicular to the wave propagation direction, respectively, to obtain the compressional and the shear wave motion. For the case of the finite

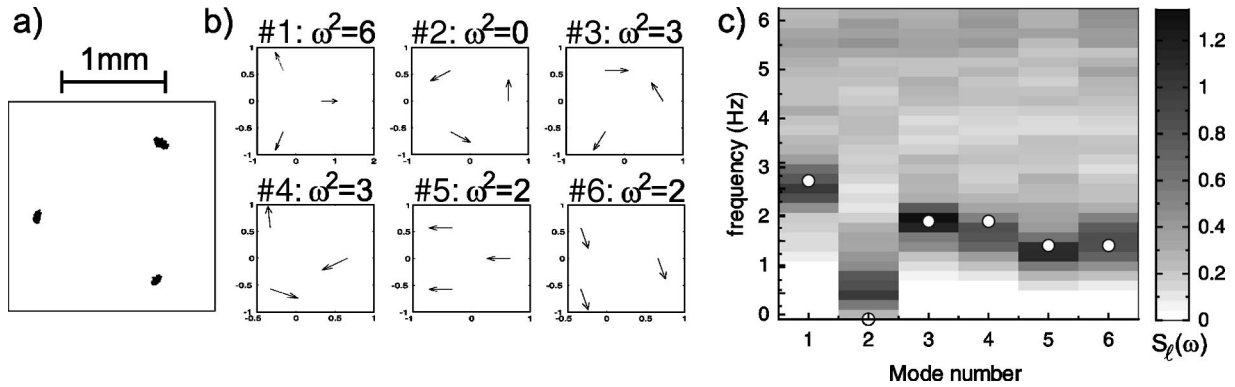

FIG. 2. Normal mode spectrum of a $N=3$ cluster. (a) Particle trajectories over 1 min. (b) Normal modes of the cluster; the indicated mode frequencies ω_ℓ^2 are normalized to $\omega_0^2/2$. (c) Measured mode spectrum of the six modes. The spectral power density is shown in gray scale. The circles correspond to the calculated mode frequencies.

clusters, here, the eigenvectors of the normal modes $\vec{e}_{i,\ell}$ take that role, since the usual wave vectors $\vec{k}_\parallel, \vec{k}_\perp$ cannot be assigned to normal modes oscillations. Consequently, the normal mode oscillations cannot be classified as pure shear or compressional modes and other methods have to be applied. We will return to that point in more detail in Sec. III D.

III. RESULTS AND DISCUSSION

We will start the presentation of the results and their discussion with the normal modes of a $N=3$ particle cluster to illustrate the technique of mode spectra obtained from the thermal particle motion. The three-particle cluster is the smallest cluster with nontrivial eigenmodes. Then, we will address the question of particle and mode temperatures as well as the properties of the particle interaction in terms of the particle charge and screening strength. After that, special attention will be paid to clusters with $N=19$ and 20 particles where we focus on specific modes, the breathing mode, and the intershell rotation. In addition, the mode with the lowest and highest excitation frequency will be analyzed for clusters with $N=3$ to $N=145$ particles. Finally, we like to gain a complete overview over all the possible modes. Therefore, the modes will be classified as either shearlike or compressionlike. This allows us to study the transition from small clusters to larger and to infinte systems.

A. $N=3$ particle cluster

First, the mode spectrum of a $N=3$ cluster is shown for a discharge power of 30 W. In Fig. 2(a) the trajectories of the three particles over 1 min are shown. One can see that the thermal fluctuations of the microspheres around their equilibrium positions are small, but they are nevertheless sufficient to determine the mode spectrum. The six eigenmodes of this cluster as calculated from Eq. (5) are depicted in Fig. 2(b). There are the following modes: the breathing mode ($\ell=1$), rotation of the entire cluster ($\ell=2$), a twofold degenerate ''kink'' mode ($\ell=3,4$), and the two sloshing modes ($\ell=5,6$). The mode frequencies ω_ℓ^2 (in units of $\omega_0^2/2$) are also indicated for $\kappa=0$.

For $\kappa>0$ the oscillation pattern of the eigenmodes is unchanged. Their frequencies, however, decisively depend on κ (see Fig. 3). As mentioned above, the frequencies of the cluster rotation ($\ell=2$, $\omega_2^2=0$) and the sloshing mode ($\ell=5,6$, $\omega_{5,6}^2=2$) are independent of κ, whereas the ''kink'' mode ($\ell=3,4$) and the breathing mode ($\ell=1$) show frequencies that increase with the screening strength. This counterintuitive result can be understood as follows. With increasing κ, the radial position r_i of the microspheres in the horizontal confinement well is reduced, the clusters become smaller due to the reduced Coulomb repulsion. With reduced distance, the curvature of the Debye-Hückel potential increases more strongly than the force, which in turn leads to the observed increase of the mode frequency.

For the three-particle cluster the dependence of the mode frequencies with screening strength looks very well behaved. However, for clusters with larger N frequency crossing of different modes can occur and the breathing mode is not the highest-frequency mode any more.

In Fig. 2(c), the measured mode spectrum is shown as a gray scale plot. Dark regions correspond to large power densities (see color bar). For comparison, the calculated mode frequencies are also indicated by the circles. One can see the very good agreement between the measured power spectrum

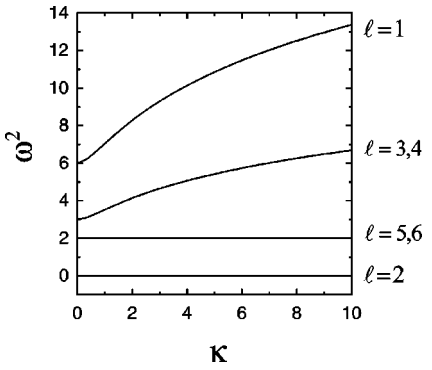

FIG. 3. Calculated mode frequencies of the three-particle cluster as a function of screening strength κ. The modes are the breathing mode ($\ell=1$), the cluster rotation ($\ell=2$), the kink modes ($\ell=3,4$), and the sloshing modes ($\ell=5,6$).

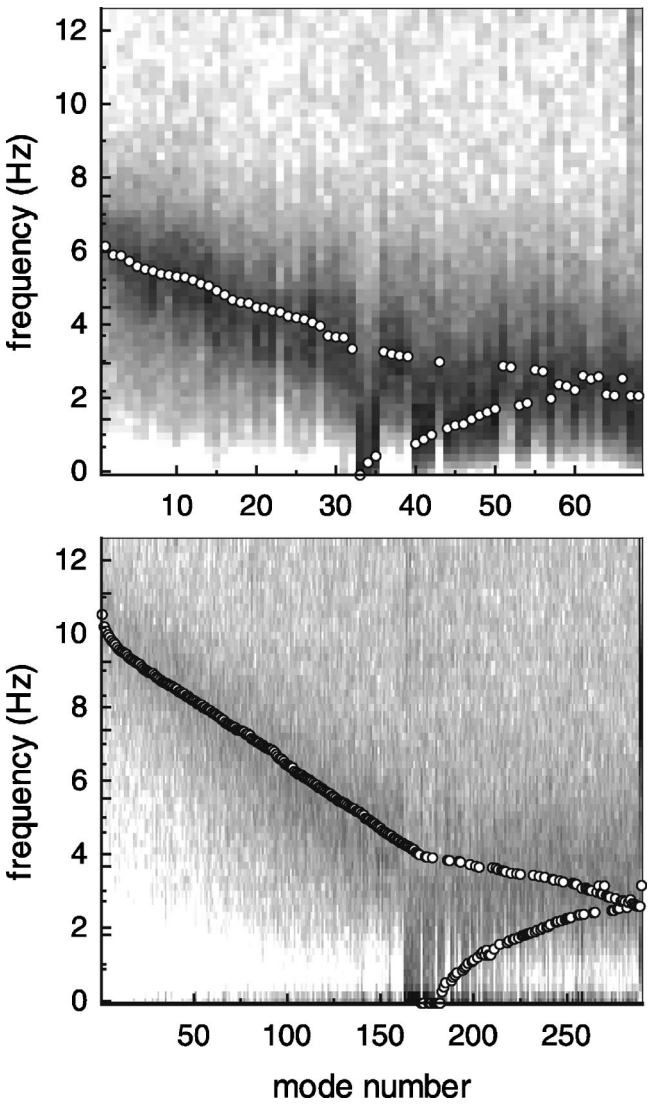

FIG. 4. Normal mode spectrum of a $N=34$ and a $N=145$ cluster. The circles correspond to the calculated mode frequencies.

and the calculated mode frequencies. Thus, the measured spectrum very well reflects the expected values.

The calculated mode frequencies can be adjusted by the two parameters screening strength κ and strength of the confinement ω_0. Agreement with the measured spectrum can be obtained in the range of $0 \leqslant \kappa \leqslant 2$. Then, the confinement strength is found to be $\omega_0/(2\pi)=1.3\pm0.2$ Hz where the error range is due to the range of κ. Using these two values and the measured particle positions, the dust charge can be extracted using the definition of r_0 in Eq. (2). The resulting dust charge of $Z=11\,000\pm1200$ varies only little with screening strength. These values are in excellent agreement with those obtained from active excitation techniques [7].

This agreement is much more convincing when looking at clusters of much higher particle numbers as shown in Fig. 4. There the measured mode spectra are shown for $N=34$ and $N=145$ particles. Again, the agreement between the measured and theoretical frequencies is very good. The resulting values of the screening strength κ and the dust charges Z are the same as for the three-particle case. Table I summarizes the particle charges obtained for the different clusters for a value of $\kappa=1$. For all cases, a particle charge close to $11\,000e$ is obtained with little variation with κ. The particle charge also does not depend significantly on the plasma power.

B. Particle and mode temperatures

First, the effective temperature of the cluster can be extracted from the normal mode spectra. We therefore make use of the relation

$$\int_0^\infty S_\ell(\omega)d\omega=\langle v_\ell^2\rangle \tag{8}$$

that yields the mean square particle velocity of mode number ℓ from the power spectrum. In a 2D system the mode temperature is related to the kinetic energy of the particles via

$$\sum_{\ell=0}^{2N}\frac{1}{2}m\langle v_\ell^2\rangle=2\frac{N}{2}kT_{\mathrm{mode},} \tag{9}$$

where the factor 2 is due to the two dimensionality of the system. Consequently, we can assign an effective temperature $T_{\mathrm{mode},\ell}=m\langle v_\ell^2\rangle/k$ to each of the modes.

For the three-particle cluster [Fig. 2(c)] it is already seen from the intensities of the gray-scale plot that the different modes seem to have comparable power densities and thus comparable temperatures. Indeed, the stored energy $kT_{\mathrm{mode}}=114$ meV is the same for each mode (within 5% error) corresponding to a temperature of $T_{\mathrm{mode}}=1318$ K. Since all the modes have the same temperature this means that the principle of equipartition is fulfilled in this case.

For comparison, the particle temperature T_{part} derived directly from the thermal motion of the particles around their equilibrium position is calculated via [9]

$$\frac{1}{2}m\langle v_{i,\alpha}^2\rangle=\frac{1}{2}kT_{\mathrm{part,i}}, \tag{10}$$

where $\alpha=x,y$ indicates the two orthogonal directions in the plane. The measured particle temperature $T_{\mathrm{part}}=1328$ K (averaged over all particles and the two directions) is very close to the mode temperature. This confirms the values obtained from the mode spectra. In this case, the measured temperature is decisively above room temperature.

These findings are substantiated from the temperature analysis of clusters with various particle numbers N. Table I also summarizes the mode and particle temperatures of the various clusters. It can be easily seen that the mode and particle temperatures are very close to each other for all investigated situations. Moreover, the temperatures are always above room temperature, varying between $T=333$ K and $T=3176$ K. Most of the clusters are found in a temperature range between 300 and 450 K. The temperatures are not correlated with particle number, interparticle distance or discharge power. Nunomura *et al.* [8] report similar particle temperatures ($440\ \mathrm{K}<T<530\ \mathrm{K}$) in a 2D extended crystal under similar conditions.

TABLE I. Mean mode temperature T_{mode} (averaged over all mode numbers $\ell=1,\ldots,2N$) and corresponding standard deviation and particle temperature T_{part} as well as dust charges Z for various particle numbers N (together with their configuration state) and discharge powers P. For clusters of $N\geqslant 58$ the indicated configuration is not strict since structural transitions occur during the measurement.

N	P/W	T_{mode}/K	T_{part}/K	Z for $\kappa=1$
3	30	1318 ± 63	1328	11 100
5	20	1104 ± 66	1122	11 000
7				
(1,6)	20	1170 ± 43	1176	10 300
12				
(3,9)	20	448 ± 60	398	11 600
12				
(4,8)	20	443 ± 62	402	11 100
16				
(1,5,10)	14	374 ± 270	391	11 200
19				
(1,6,12)	35	333 ± 62	387	10 200
19				
(1,7,11)	3	354 ± 86	467	13 700
20				
(1,7,12)	40	760 ± 2000	662	7 500
34				
(1,6,12,15)	23	3167 ± 925	2886	11 400
38				
(2,8,13,15)	23	554 ± 161	535	12 100
58				
(1,7,13,18,19)	47	684 ± 405	575	11 300
59				
(2,7,13,18,19)	16	396 ± 131	371	11 300
145				
(1,6,12,18,24,25,28,31)	32	349 ± 143	408	10 900

The observed additional heating above room temperature is assumed to be due to stochastic charge and electric field fluctuations which can lead to significant increase of temperature [10].

C. Analysis of special modes

In this section, we will focus on special type of modes and will compare their behavior among different particle cluster numbers and with theoretical predictions.

1. Breathing mode and intershell rotation

First, we analyze the breathing mode and intershell rotation. As mentioned above, the breathing mode is a purely radial coherent oscillation of all particles that is independent of particle number at $\omega_{\mathrm{b}}=\sqrt{3}\omega_0$ for pure Coulomb interaction. With increasing κ, the frequency of this mode increases and very weakly depends on particle number. The intershell rotation is a mode where inner and outer rings rotate with respect to each other. We will dwell on these modes for the specific case of $N=19$ and 20 particles. We thus revisit the

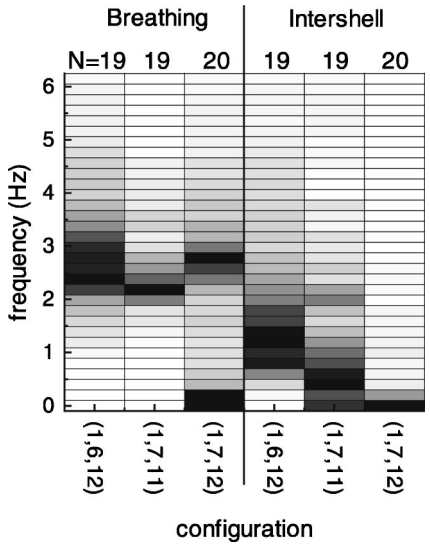

FIG. 5. Mode spectra of of the breathing and intershell rotation mode for $N=19$ in (1,6,12) and (1,7,11) configuration as well as for the $N=20$ (1,7,12) cluster.

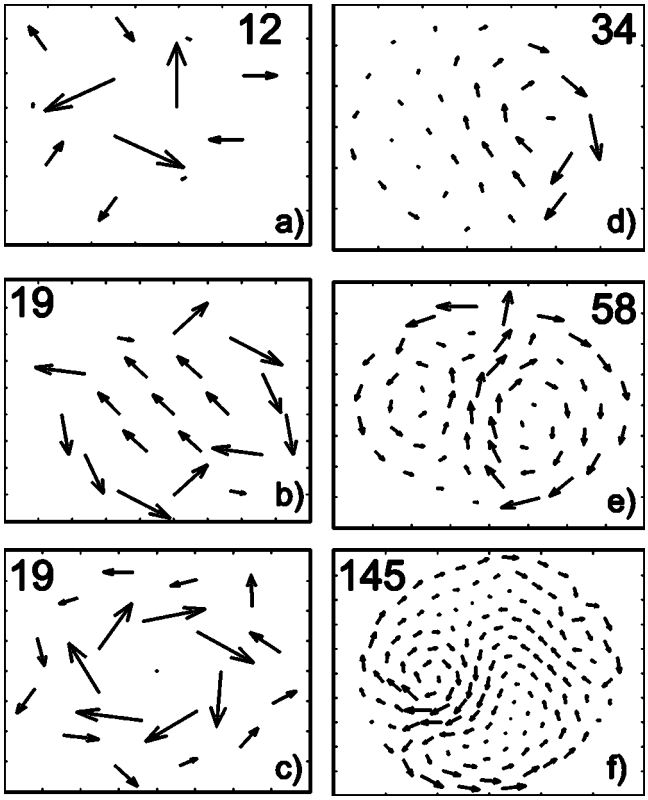

FIG. 6. Modes of lowest frequency obtained from the thermal mode spectra for (a) 12 particles (3,9), (b) 19 (1,6,12), (c) 19 (1,7,11), (d) 34, (e) 58, and (f) 145 particles.

investigations of Klindworth *et al.* [6], who have intentionally driven the intershell rotation by a pair of laser beams in exactly this cluster pair.

This cluster pair has special interesting characteristics: Due to the commensurate number of particles in the inner and outer rings (6 and 12, respectively) and the sixfold symmetry the $N=19$ (1,6,12) particle cluster is extremely stable against intershell rotation and, thus, intershell mode frequency should be relatively high. The $N=20$ (1,7,12) cluster has an incommensurate number of particles in the two rings. Intershell rotation should be easily excited. It is therefore expected that the corresponding mode frequency is small. In addition, the 19-particle cluster has a metastable state with a (1,7,11) configuration that is similar to the 20-particle system with an associated low-frequency intershell rotation. For pure Coulomb interaction the intershell rotation is the mode with lowest frequency (besides the simple rotation of the entire cluster around the symmetry axis at $\omega=0$) for $N<39$ [3].

The experimental results of the breathing mode and the intershell rotation for the three cluster configurations are shown in Fig. 5. It is seen that the breathing mode is found at $\omega_b/(2\pi)=2.5\pm0.2$ Hz for all three clusters. With the value for the sloshing mode of $\omega_0/(2\pi)=1.3$ Hz this results in $\omega_b/\omega_0=1.9\pm0.4$ or in normalized units $\omega_b^2=7.22\pm3$. The theoretical normalized frequency is $\omega_b^2=7.4$ at $\kappa=1$ (compare the frequency of the breathing mode of the three-particle cluster in Fig. 3). However, due to the error range a screening strength of $\kappa=0-5$ is compatible with the experiments.

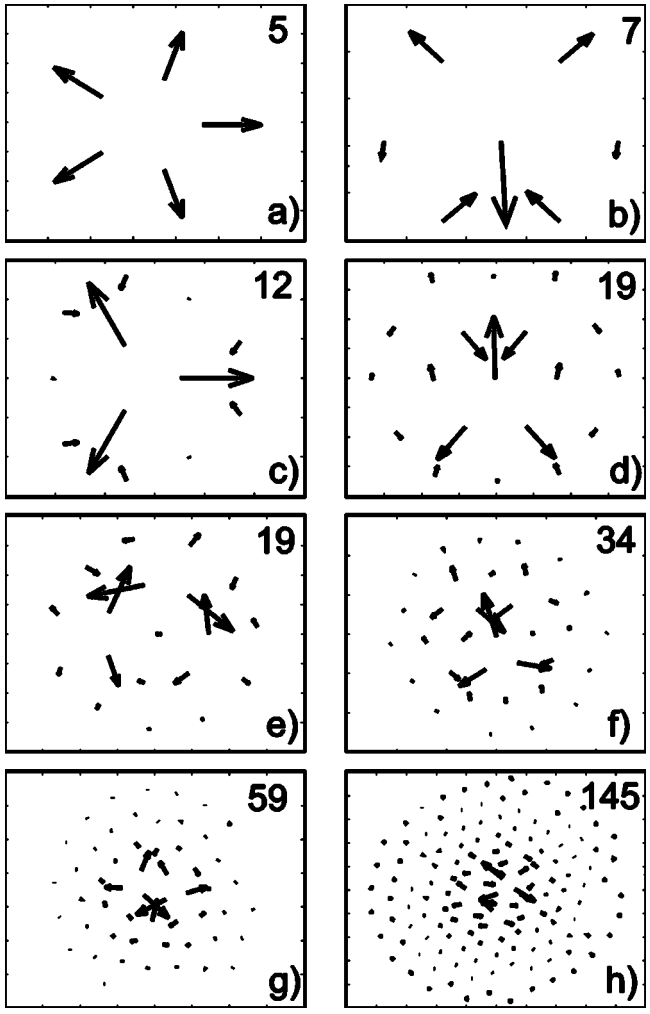

FIG. 7. Modes of highest frequency obtained from the thermal mode spectra for (a) 5, (b) 7, (c) 12 (3,9), (d) 19 (1,6,12), (e) 19 (1,7,11), (f) 34, (g) 59, and (h) 145 particles.

The intershell rotation mode shows a peak at about 1.2 Hz for the highly ordered 19-particle cluster, whereas the incommensurate cluster configurations show peaks below 0.5 Hz. This confirms the above described behavior of these clusters with a high intershell rotation frequency for the ordered, commensurate (1,6,12) cluster and the low frequency for the incommensurate $N=19$ (1,7,11) and $N=20$ (1,7,12) structures. This is also in very good agreement with the laser excitation of the intershell rotation [6]. These experiments verify the strong dependence of mode frequencies on cluster configuration.

2. Lowest-frequency modes

In this section, we wish to address the question of the lowest-frequency modes (LFMs) apart from the simple rotation at $\omega=0$. Since we are able to extract *all* modes of a particular cluster from the thermal mode spectra, the LFMs can be identified in the experiment. From simulations in clusters with pure Coulomb interaction [3], it is found that

clusters with a small number of particles exhibit intershell rotation, whereas for higher particle numbers the formation of vortex-antivortex pairs is found as the LFMs.

Here, the LFMs are obtained for different particle numbers from the measured thermal mode spectra. For that purpose, the mean frequencies weighted by the spectral power density of all modes are calculated,

$$\overline{\omega}_\ell = \frac{\int \omega S_\ell(\omega) d\omega}{\int S_\ell(\omega) d\omega}, \tag{11}$$

and the minimum frequency (besides simple rotation) is identified. The resulting lowest-frequency modes are shown in Fig. 6 for different cluster sizes. Intershell rotation is indeed found as the LFM for 12 particles, both in the (3,9) [see Fig. 6(a)] and (4,8) configuration (not shown), and for 19 particles in the incommensurate configuration (1,7,11) [see Fig. 6(c)].

For the $N=19$ (1,6,12) configuration, the formation of a vortex-antivortex pair is observed [Fig. 6(b)]. This is unexpected, since for pure Coulomb interaction, intershell rotation is the LFM also in this configuration [3]. However, the vortex-antivortex pair becomes the LFM for finite values of κ. This is due to the fact that with the ''harder'' interparticle potential at finite κ the inner and outer rings are nested more tightly and thus the corresponding intershell rotation frequency becomes higher and the vortex-antivortex formation is obtained as the LFM.

For 34, 58, and 145 particles, Fig. 6(d), 6(e), and 6(f) also the vortex-antivortex pair is found. In some of these cases (34 and 145 particles) unexpected asymmetries between the two vortices can be observed. This is certainly due to the fact that the clusters in the experiment do not show perfect order and even slight deviations cause differences in the mode structure. The formation of vortex-antivortex pairs is commonly found as a very stable configuration in fluids. Thus larger clusters behave in some respects as incompressible fluids.

That intershell rotation and vortex-antivortex structures are associated with extremely low frequencies becomes clear when realizing that these mode patterns minimize the relative motion of neighboring particles. With only little relative particle motion the restoring forces are small and the mode frequencies are low. At higher particle numbers it becomes more favorable not to maintain the rotation of entire concentric rings of the cluster, but rather to split into two rotations around eccentric points, thus establishing the vortex-antivortex motion.

3. Highest-frequency mode

In a similar manner, also the highest-frequency modes (HFMs) have been obtained from the mode spectra. The HFMs as obtained from the experiment are presented in Fig. 7. As already mentioned above, the breathing mode is the HFM only for very small clusters, i.e., for particle numbers $N \leqslant 5$ in our experiments. Already for the seven-particle cluster the HFM is characterized by a localized relative motion of three particles [the lower three particles in Fig. 7(b)]. Such a motion involves a strong change of interparticle distance resulting in strong restoring forces and thus a high frequency of the mode. This localized three-particle motion is clearly observed for the other clusters of higher particle number. This becomes particularly obvious in the 12-particle cluster with its threefold symmetry. In the clusters with higher particle numbers, i.e., $N \geqslant 34$, it is seen that the strongest relative particle motion is concentrated in the inner two rings only. The outer rings are more or less motionless.

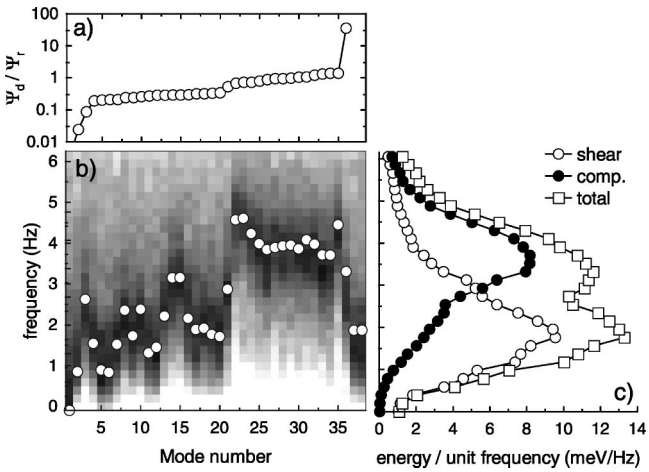

FIG. 8. Thermal mode spectra of the $N=19$ (1,6,12) cluster (b). Here, the modes are ordered according to the ratio of Ψ_d/Ψ_r. The corresponding values of Ψ_d/Ψ_r are shown in the upper plot vs the respective mode number (a). The right panel shows the spectrum integrated over the different modes (c). Here, ''total'' corresponds to the summation over all 38 modes, whereas ''shear'' corresponds to the sum over the 18 modes with the low Ψ_d/Ψ_r ratio, and ''compressional'' to that with the high ratio.

Again, the 19 (1,6,12) cluster plays an interesting role here. The mode that is identified as the HFM from the experiments [see Fig. 7(d)] is not the mode of highest frequency from the calculations with pure Coulomb interaction. It becomes, however, the calculated highest frequency mode for κ larger than a critical value of κ of about 1. This is another indication that the screening strength has a finite value in these systems.

D. Shearlike and compressionlike modes

Finally, to gain overall insight into the behavior of the cluster modes they will be classified as shearlike or compressionlike modes here. In a two-dimensional infinite lattice two types of waves can propagate, the compressional mode and the shear mode, where the particle displacement of the wave oscillation is along or perpendicular to the wave vector, respectively. The compressional mode does not involve any rotational motion, thus $\vec{\nabla} \times \vec{v} = 0$ for the particle velocities $\vec{v}$ of this mode. Analogously, the shear mode conserves the particle density and, therefore, $\vec{\nabla} \cdot \vec{v} = 0$ for the shear wave. Consequently, the compressional (shear) properties can be extracted from the divergence (rotor) of the velocity field.

This technique has been applied, e.g., to the identification of shear and compressional Mach cones in plasma crystals [11,12].

Due to the circular boundary of clusters, pure shear or compressional modes do not exist there. However, the above procedure can also be applied to clusters in order to separate the compressional and shear contributions of each mode. This can be done by calculating the divergence $\Psi_d(\ell) = \mathrm{div}\,\Psi(\ell)$ and the z component of the rotor $\Psi_r(\ell) = \vec{e}_z \cdot \mathrm{rot}\,\Psi(\ell)$ of the field of eigenvectors Ψ for the different modes [3]:

$$\Psi_d(\ell)^2 = \frac{1}{N}\sum_{i=1}^{N} \psi_{d,i}^2(\ell), \tag{12a}$$

$$\Psi_r(\ell)^2 = \frac{1}{N}\sum_{i=1}^{N} \psi_{r,i}^2(\ell), \tag{12b}$$

where

$$\psi_{d,i}(\ell) = \frac{1}{M}\sum_{m=1}^{M} (\vec{r}_i - \vec{r}_m)\cdot[\vec{e}_i(\ell) - \vec{e}_m(\ell)]/|\vec{r}_i - \vec{r}_m|^2,$$

$$\psi_{r,i}(\ell) = \frac{1}{M}\sum_{m=1}^{M} |(\vec{r}_i - \vec{r}_m)\times[\vec{e}_i(\ell) - \vec{e}_m(\ell)]|/|\vec{r}_i - \vec{r}_m|^2.$$

Here, m,M denote the index and number of neighboring particles to particle i. Thus, $\Psi_d(\ell)$ is the magnitude of the compressional contribution to mode ℓ, and $\Psi_r(\ell)$ to its shear part. For the two sloshing modes, $\Psi_d = \Psi_r = 0$ since they do not involve any kind of relative motion. The mode with the highest Ψ_d/Ψ_r ratio is the breathing mode and that with the lowest is the simple rotation around the central axis followed by the intershell rotation for small particle numbers N.

1. Mode-integrated spectra

We start the discussion of shearlike and compressionlike modes with the already widely discussed $N=19$ (1,6,12) cluster. Figure 8(b) shows the thermal mode spectrum of this cluster, where the modes have been ordered according to their Ψ_d/Ψ_r ratio. The Ψ_d/Ψ_r ratio versus the mode number is indicated in Fig. 8(a). It is seen that typical values for the compression-to-shear ratio lie in the range between $\Psi_d/\Psi_r = 0.1$ and 2. Only the first mode (the simple rotation) and the last ''regular'' mode, number 36 (breathing mode), have a much lower and higher value, respectively. The last two mode numbers (37 and 38) have been assigned to the two sloshing modes that do not have a defined Ψ_d/Ψ_r ratio.

In Fig. 8(c) the thermal spectrum integrated over the mode number, i.e., $S(\omega) = \Sigma S_\ell(\omega)$, is presented. The ''total'' $S(\omega)$ spectrum, which is obtained by summation over all the 38 modes, shows a decisive double-peak structure with peaks at about $f = 1.8$ Hz and $f = 3.4$ Hz. Such a double-hump spectrum is also seen in infinite'' 2D crystals where the peak of higher (lower) frequency was attributed to the compressional (shear) mode [13]. Thus, it can be speculated that also for the finite clusters the high-frequency peak is due to the more compression-like modes and the low-frequency peak due to shear-like modes.

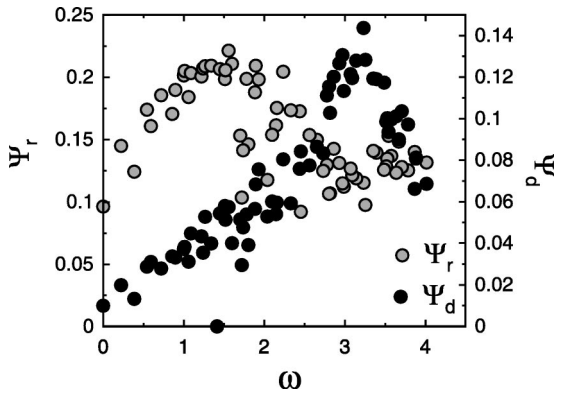

FIG. 9. Distribution of the rotor Ψ_r and the divergence Ψ_d as a function of the normalized frequency for the 68 modes of a $N = 34$ particle cluster.

In order to check this conjecture the mode spectrum was summed over two different regions, the first 18 modes with the lowest Ψ_d/Ψ_r ratio, which correspond to the more shear-like modes, and the second 18 modes with the highest Ψ_d/Ψ_r ratio, which are more compressionlike (note that the two sloshing modes with undefined ratio are not considered here). The result is shown in Fig. 8(c). It is clearly seen that the ''shear'' modes form the low-frequency peak and the ''compressional'' modes establish the high-frequency peak. There is a clear separation between these two mode populations. This is already obvious from the thermal mode spectrum, where the first 18 modes have low frequencies and the second 18 modes (mode 19 to 36) clearly show a separated regime with high frequencies.

Such a double-peak spectrum $S(\omega)$ is found for all cluster sizes $N \geqslant 5$, for the three-particle cluster a definite answer cannot be given. However, the clearly separated shear and compressional population is observed only for larger clusters with 12 particles and more. For the smaller clusters ($N \leqslant 7$) the shear and the compressional contributions are alike and more evenly distributed over the frequency range. It can thus be argued that crystal-like properties in the cluster arise when the cluster is larger than a critical particle number which is between 7 and 12 from these experiments.

2. Transition to ''infinite'' systems

The above finding of the relation between the critical cluster size and the infinite lattice leads us to the question of how the transition of a finite cluster to an infinite crystal takes place in the view of the normal modes and waves in these systems. At high particle numbers the normal modes of a finite cluster system must merge into the dispersion relation of shear and compressional modes of a 2D lattice. This question has been addressed here using the example of the cluster with $N = 34$ particles.

First, the distribution of the rotor Ψ_r and the divergence Ψ_d as a function of the calculated normalized frequency ω is given in Fig. 9. It is seen that the rotor has quite large values

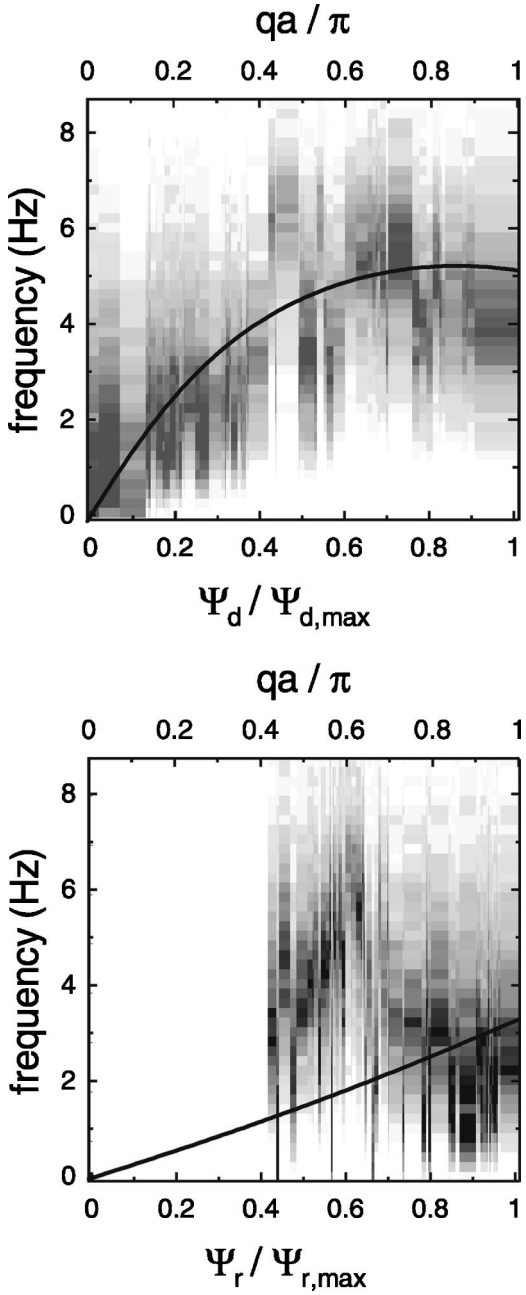

FIG. 10. Mode spectrum of a cluster with 34 particles as a function of its effective compressional and shear wave number (i.e., $\Psi_d/\Psi_{d,max}$ and $\Psi_r/\Psi_{r,max}$). For comparison the dispersion relation of the compressional and shear wave in an ''infinite'' 2D crystal with $\kappa=1$ is also given as a function of qa/π (solid line).

at low frequencies with a broad maximum around $\omega=1.5$ and then gradually drops with increasing frequency. In contrast, the divergence is very small at low frequencies and increases to a maximum around $\omega=3.2$. These two maximum frequencies coincide with the shear and compression maxima of the double-humped integrated mode spectrum $S(\omega)$. From this figure, it also becomes obvious that higher Ψ_d/Ψ_r ratios (the more compressional modes) are found at higher frequencies. The fact that at low-frequencies the rotor is much larger than the divergence means that the system is incompressible and that low frequency excitations are vortexlike motions where the particle density is undisturbed [3] which is also seen from the discussion on the LFMs in Sec. III C 2.

To attack the transition from normal modes to a 2D dispersion relation, it is necessary to assign an effective wave number to each cluster mode. This can be done using the rotor and divergence. In plasma wave physics, the rotor (and divergence) operator is straightforwardly replaced by the wave vector in Fourier notation (i.e., $\vec{\nabla}\times\cdots\rightarrow i\vec{q}\times\cdots$). Consequently, it is proposed here to identify the rotor Ψ_r with the wave number of the shear wave and the divergence Ψ_d with that of the compressional wave.

Figure 10 shows the mode spectrum of the $N=34$ particle cluster where the spectrum has been ordered according to the wave number of the compressional mode $\Psi_d/\Psi_{d,max}$ and the shear mode $\Psi_r/\Psi_{r,max}$, respectively (here, $\Psi_{r,max},\Psi_{d,max}$ are the maximum values of Ψ_r,Ψ_d, respectively). For comparison, the dispersion of the compressional and shear mode of the 2D lattice wave with $\kappa=1$ is also shown. For the calculation of the theoretical 2D dispersion the quantities as obtained from the experiment have been used. The theoretical dispersion scales with the dust plasma frequency

$$\omega_{pd}=\sqrt{\frac{Z^2e^2}{4\pi\epsilon_0 ma^3}}=11.4\ \mathrm{s}^{-1}$$

for a charge number of $Z=11\,000$ and an interparticle distance of $a=680\ \mu$m.

It is seen that the agreement between the normal mode ''dispersion'' and the lattice wave is quite remarkable for the compressional mode. Note that this comparison does not include any adjustable parameters. For the shear modes the agreement is quite good for the higher wave numbers $\Psi_r/\Psi_{r,max}>0.7$. At medium wave numbers $0.4<\Psi_r/\Psi_{r,max}<0.7$ a branch with somewhat higher mode frequencies exists that is not explained by this comparison. Very similar results with a very good agreement of normal modes with the wave number and the 2D lattice dispersion are also found for other clusters, e.g., $N=19$ and $N=145$.

It seems that this *ad hoc* assignment of the rotor and the divergence to shear and compressional wave vectors is a good working model that indeed can relate the cluster normal modes to the wave propagation in a 2D lattice. However, a theoretical treatment of this scenario has to be developed.

IV. SUMMARY AND CONCLUSIONS

Experiments on the normal modes of 2D finite Coulomb clusters in a complex plasma have been performed. The normal modes have been obtained from the thermal Brownian motion of the particles around their equilibrium positions in the cluster. This technique thus extends the thermal excitation technique of Nunomura *et al.* [8] in a 2D lattice to the case of Coulomb clusters. This technique has been illustrated with the simple case of a three-particle cluster and has been applied to various cluster sizes and cluster configurations under different discharge conditions. It has been found that

the energy in the modes is evenly distributed among the modes, thus the principle of equipartition holds here. The temperature deduced from the mode energies varies between 300 K and 3000 K. The additional heating above room temperature is assumed to be due to stochastic fluctuations of discharge parameters. The mode temperature is also in excellent agreement with the temperature directly obtained from the random fluctuations of the particles around their equilibrium.

From the analysis of the normal mode frequencies the interaction between the particles can be described by a Yukawa interaction with a screening strength κ between 0 and 2 and particle charges of $Z=11\,000$ elementary charges. These values are in perfect agreement with previous mode excitation measurements [7] and also direct wave excitation by laser techniques [14–16], and two-particle collision experiments [17].

Since the thermal motion technique allows to determine all cluster modes simultaneously the behavior of special modes can be compared in different cluster sizes and configurations. First, the breathing mode and intershell rotation have been analyzed for the 19- and 20-particle clusters where the 19-particle cluster can have either a ''magic number'' or an incommensurate configuration that is similar to the 20-particle system. It has been found that the breathing mode spectrum shows very similar frequencies for these cluster configurations, whereas the intershell rotation frequency is highest for the highly symmetric 19 cluster and close to zero for the two incommensurate configurations. This clearly shows the strong relation between cluster configuration and normal mode frequencies.

Second, the modes with the lowest frequency have been identified for different cluster sizes. For small particle numbers the intershell rotation has been identified as the LFM, whereas for larger clusters the formation of vortex-antivortex pairs were observed. This behavior is generally within the theoretical expectations for pure Coulomb systems [3]. The 19-particle cluster, however, is an exception in that here the vortex-antivortex formation instead of intershell rotation was found. This requires a ''harder'' interaction potential than pure Coulomb which hints at finite values of the screening strength, i.e., $\kappa>0$.

Third, also the highest-frequency modes have been analyzed. For small clusters, the breathing mode with a coherent radial motion of all particles is the HFM. For larger clusters, modes with a relative three-particle oscillation localized in the center of the cloud provide the highest frequencies. Again, from the behavior of the $N=19$ cluster, the screening strength can be estimated to be $\kappa>1$.

Finally, the modes have been classified as shearlike or compressionlike using the rotor and the divergence of the individual cluster modes. It is observed that all clusters show a double-humped mode-integrated frequency spectrum $S(\omega)$. For clusters with 12 particles or more the high-frequency peak is due to the compressional modes and the low-frequency peak due to the shear modes. Thus, it can be argued that crystal properties become visible or dominant at cluster size of $N\geqslant 12$.

The transition from clusters to continuum 2D crystals can also be studied from the comparison of the normal mode spectra with lattice waves. Therefore, a shear and compressional wave number has been assigned to the different modes. In doing so, a dispersion of compressional and shear normal modes has been obtained. This normal mode dispersion has been compared to the dispersion relation of lattice waves and a remarkably good agreement has been observed. In conclusion, this wave number assignment seems to be a working model to relate the finite cluster modes to the continuum lattice waves.

ACKNOWLEDGMENTS

Helpful discussions with I. Schweigert (Novosibirsk), F. Peeters (Antwerp) as well as with M. Klindworth and A. Piel (both University Kiel) are gratefully acknowledged.

[1] A. Piel and A. Melzer, Plasma Phys. Controlled Fusion **44**, R1 (2002).
[2] V.M. Bedanov and F. Peeters, Phys. Rev. B **49**, 2667 (1994).
[3] V.A. Schweigert and F. Peeters, Phys. Rev. B **51**, 7700 (1995).
[4] Y.-J. Lai and L. I, Phys. Rev. E **60**, 4743 (1999).
[5] W.-T. Juan *et al.*, Phys. Rev. E **58**, 6947 (1998).
[6] M. Klindworth, A. Melzer, A. Piel, and V. Schweigert, Phys. Rev. B **61**, 8404 (2000).
[7] A. Melzer, M. Klindworth, and A. Piel, Phys. Rev. Lett. **87**, 115002 (2001).
[8] S. Nunomura *et al.*, Phys. Rev. Lett. **89**, 035001 (2002).
[9] A. Melzer *et al.*, Phys. Rev. E **54**, 46 (1996).
[10] R. Quinn and J. Goree, Phys. Rev. E **61**, 3033 (2000).
[11] V. Nosenko, J. Goree, Z.W. Ma, and A. Piel, Phys. Rev. Lett. **88**, 135001 (2002).
[12] Z.W. Ma and A. Bhattacharjee, Phys. Plasmas **9**, 3349 (2002).
[13] S. Nunomura, D. Samsonov, and J. Goree, Phys. Rev. Lett. **84**, 5141 (2000).
[14] A. Homann *et al.*, Phys. Rev. E **56**, 7138 (1997).
[15] A. Homann, A. Melzer, R. Madani, and A. Piel, Phys. Lett. A **242**, 173 (1998).
[16] A. Melzer, Plasma Sources Sci. Technol. **10**, 303 (2001).
[17] U. Konopka, G. Morfill, and L. Ratke, Phys. Rev. Lett. **84**, 891 (2000).